Received: 30 May 2024 | Revised: 3 August 2024 | Accepted: 6 August 2024

DOI: 10.1002/apj.3144

RESEARCH ARTICLE

Asia-Pacific Journal of Chemical Engineering | Curtin University | WILEY

ZnO-doped kaolin nanoclay immobilized agar biopolymer for 2,4-dinitrophenol photocatalytic degradation

Imran Hasan[1] | **Akshara Bassi**[2] | **Parvathalu Kalakonda**[3] | **Kushal Kanungo**[2]

[1]Department of Chemistry, College of Science, King Saud University, Riyadh, 11451, Saudi Arabia

[2]Environmental Research Lab, Department of Chemistry, Chandigarh University, Mohali, Punjab, 140413, India

[3]Dept of Physics, Smart Nano Materials Research Laboratory, Government City PG College Autonomous, Osmania University, Hyderabad, Telangana, India, 50002

Correspondence
Imran Hasan, Department of Chemistry, College of Science, King Saud University, Riyadh 11451, Saudi Arabia.
Email: iabdulateef@ksu.edu.sa

Funding information
King Saud University, Grant/Award Number: RSPD2024R670

Abstract

This study focuses on enhancing the properties of kaolin (Kao) clay by incorporating Zinc oxide nanoparticles (ZnO NPs) and further functionalizing with agar biopolymer, resulting in the formation of Agar/Kao@ZnO nanocomposite (NC). The synthesized material underwent comprehensive composition, structure, surface, and optical properties analysis to confirm the formation. The material was evaluated as a photocatalyst for the degradation of 2,4-dinitrophenol (DNP) under visible light irradiation. The optimized conditions for the photocatalytic degradation of DNP were determined as irradiation time 50 minutes, pH 4, catalyst dose 20 mg, and DNP concentration of 25 mg L^{-1}, resulting in degradation efficiency of 99.63%. Trapping experiment validated the significant role of hydroxyl ($^{\bullet}OH$) radicals as reactive oxidant species (ROS) in the degradation of DNP in the presence of visible light. Through four consecutive cycles of reusability experiments, it was confirmed that the synthesized material is highly stable and efficient for DNP degradation.

KEYWORDS

2,4-dinitrophenol, biopolymer, nanoclay, nanocomposite, photocatalytic degradation, ZnO

1 | INTRODUCTION

The presence of organic and inorganic pollutants in water has significant economic and environmental consequences, leading to the generation of toxic effluents.[1,2] Among the plethora of carcinogenic and mutagenic compounds found in water sources, nitrophenols and its derivatives, especially 2,4-dinitrophenol (DNP), are particularly toxic pollutants discharged by various industries including agriculture, pharmaceutical, manufacturing, etc.[3,4] The excessive accumulation of DNP in industrial waste, soil, and aquatic ecosystems poses serious threats due to its high solubility in water, propensity to bioaccumulate, and serve toxicity, which can lead to mutations and genetic damage.[5–7] The robust stability of DNP, its resistance to natural breakdown processes, and concerns about generating harmful by-products present challenges to its removal.[8,9] The predominant technology for addressing organic pollutants involves adsorption, but it suffers from drawbacks such as inefficiency, time-intensive procedures, and substantial investment requirements.[10] Furthermore, it is essential to evaluate the ecological impact on water bodies after DNP removal to ensure a sustainable ecosystem.[11–13]

Among various methods, photocatalysis stands out as one of the most effective techniques based on advanced oxidative processes (AOPs), utilizing renewable and clean solar energy to completely mineralize the organic pollutants.[5] Photocatalysis offers economic and eco-friendly advantages, being highly efficient, non-toxic, and chemically stable.[6,7] Importantly, it avoids the production of secondary pollution after treatment reactions.[8–10] In this method, the catalyst's surface interacts with light, leading to the excitation of the electrons from valence band

(VB) to conduction band (CB), generating electron–hole pairs. These electron–hole pair interact with oxygen and water in the system, producing hydroxyl ($^{\bullet}OH$) and superoxide ($^{\bullet}O_2^-$) radicals.[11] These radicals subsequently attack the pollutant molecules, mineralizing them into smaller, non-toxic entities.[12]

Semiconductor-based nanomaterials have been widely employed as photocatalysts for pollutants degradation due to their ability to absorb radiation and generate electron–hole pair.[13] Various semiconductors-based nanomaterials, including TiO_2, MnO_2, ZnO, SnO_2, CdO, etc., have been investigated for the degradation of different organic pollutants. Among these, ZnO is particularly noteworthy as n-type semiconductor with a wide range of applications in UV lasers, gas sensing, and solar cells.[14] It possesses excellent photocatalytic properties, non-toxicity, abundance, and a high aspect ratio, with a band gap value of 3.4 eV.[15,16] ZnO NPs exhibit a hexagonal wurtzite structure, facilitating anisotropic nucleation of NPs for the large amount of photoinduced e^-/h^+ pair on or near catalyst surface.[17] However, ZnO NPs encounter challenges in their photocatalytic properties, such as a high bandgap that restricts their response to only UV region of sunlight constituting a small fraction (5–7%) of the total solar spectrum[18,19]. Another limitation is the high rate of electron–hole pair recombination rate.[20] To address these issues, various modification methods have been applied, including doping with metal and non-metals, composite formation, and surface modification. One such approach involves the dispersion of pristine ZnO NPs in kaolin nanoclay as a medium, followed by surface modification by agar gum biopolymer.

Clays are naturally occurring materials characterized by layers of aluminosilicates, divided into two categories; pillared clays and non-pillared clays.[21,22] Among these, Kaolin, with chemical formula of ($Al_2Si_2O_5[OH]_4$), is a 1:1 layered type of clay material found in nature. It consists of $Al_2(OH)_4$ and SiO_4, with octahedral and tetrahedral sheets, respectively.[23] Kaolin serves as a host material and exhibits effective adsorption due to its cationic exchange capacity, ability to swell in the aqueous solution, and large surface area with environmental stability.[20,24–26] The hydrophilic groups present on the surface of kaolin and the covalent bonds between layers effectively immobilize the ZnO NPs, providing stability. In synergy, ZnO NPs act as sensitizer extending the photoresponsivity of the synthesized nanocomposite material.[22,27] Furthermore, to improve the surface functional density and biocompatibility of Kao@ZnO, surface functionalization using biopolymers such as chitosan, sodium alginate, agar, xanthan gum has garnered extensive attention.[28] Agar gum ($C_{12}H_{18}O_9$), a linear polysaccharide derived from red seaweeds such as Gracilaria and Gelidium, is composed of D-galactose and 3,6-anhydro-β-galactopyranose units.[29,30] Widely utilized as a stabilizer, thickener and gelling agents in various industries including cosmetics, microbiology and food industries, agar gum offers valuable properties for numerous applications.[31,32] The hydroxyl (-OH) groups within the biopolymer play a crucial role in facilitating the adhesion of organic pollutants onto the catalyst's surface through the formation of electrostatic or covalent bonds.[33]

The current study showcases the synthesis of nanocomposite (NC) wherein ZnO NPs are incorporated into a Kaolin matrix and immobilized by agar biopolymer. This novel material was investigated as a photocatalyst for the degradation of DNP. Several influential parameters, including irradiation time, pH, catalyst dose, and initial dye concentration, were optimized, and the kinetics of the reaction were briefly discussed.

2 | METHODS AND METHODS

2.1 | Chemicals and reagents used

Zinc nitrate Zn $(NO_3)_2.6H_2O$ in the form of white crystals AR grade was purchased from Merck India. Agar gum and Kaolin were supplied by Fluka, India. 2,4-Dinitrophenol, with a maximum absorbance in the range of λ_{max} = 350–360 nm, was purchased from Sigma-Aldrich, India. Potassium hydroxide (KOH) was obtained from Sigma Aldrich, India. The precise quantities of salts and reagents were dissolved in double-distilled water to prepare the stock solutions.

2.2 | Synthesis of Agar/Kao@ZnO NC

The material synthesis involved an in situ chemical co-precipitation method combined with the sol–gel method.[31] The detailed method is as follows: A 5% (w/V) solution of agar gum was prepared by mixing 5 g of agar biopolymer in 100 ml of distilled water, followed by stirring until complete dispersion was achieved. Simultaneously, in another flask, 5 g of kaolin was mixed with 100 ml of 2 M of Zn $(NO_3)_2$ solution and subjected to ultrasonicated for better suspension. The kaolin suspension in the Zn $(NO_3)_2$ solution was gradually added dropwise to the agar biopolymer solution, and the mixture was stirred until homogeneity was attained in the biopolymer blend. Subsequently, 30 ml of 0.4 M KOH solution was added and the product was collected through vacuum pump filtration. The resulting product was washed multiple times with distilled water to remove any undesired particles and then dried in a hot air oven at 60°C for 6 hrs.

2.3 | Characterisation of Agar/Kao@ZnO NC

To comprehensively analyze the crystal structure, morphology, bonding, and functional groups of the Agar/Kao@ZnO NC, various instrumental techniques were employed. Fourier transform infrared spectroscopy (FTIR) using a Perkin Elmer (PE1600) instrument within the range of 400–4,000 cm^{-1} was utilized to determine the bonding and functional groups present in the material. X-ray Diffraction (XRD) analysis was performed using a Rigaku Ultima 1 V X-ray diffractometer with Cu Kα radiation (λ = 1.540 Å) to obtain information regarding lattice and crystal size, aiding in understanding the blending of individual constituents. The surface morphology and chemical composition of the material were assessed using scanning electron microscope SEM (GSM 6510LV, JEOL) coupled with energy dispersive X-ray (EDX) analysis to calculate the homogeneity. Transmission electron microscope (TEM) analysis using a JEM, 2100 instrument was employed to determine the size of particles dispersed within the biopolymer and nanoclays matrix. The specific surface area of the synthesized material was evaluated using a Micromeritics Tristar II, and values were determined using the Brunauer–Emmett–Teller method (BET) method. The concentration of pollutants, i.e., 2,4-DNP before and after photocatalytic reaction, as well as the optical properties of synthesized material, were examined by UV–Vis double beam spectrophotometer Shimadzu (UV-1900).

2.4 | Photocatalytic experiment

The photocatalytic degradation experiment of 2,4-dinitrophenol (DNP) using Agar/Kao@ZnO NC was conducted via the batch method under a visible light source, i.e., halogen lamp of 50 W. The distance between radiation source and solution was 25 cm. For each experiment, an aliquot of 25 ml of 2,4-DNP was prepared for different concentrations (10–50 mgl^{-1}) solution, pH (4, 6, 8, and 10), catalyst dose of 10–20 mg and irradiation time (10–50 min) in the presence of visible light source. After each experiment, the optimized values of each parameter were determined and utilized for kinetics and scavenger tests. The photocatalyst efficiency was analyzed by using a UV–Vis spectrophotometer at a maximum absorption wavelength of DNP at λ_{max} = 358 nm. The extent of % degradation was calculated by using the equation:

$$\text{Degradation}\,(\%) = \frac{C_i - C_t}{C_i} \times 100 \qquad (1)$$

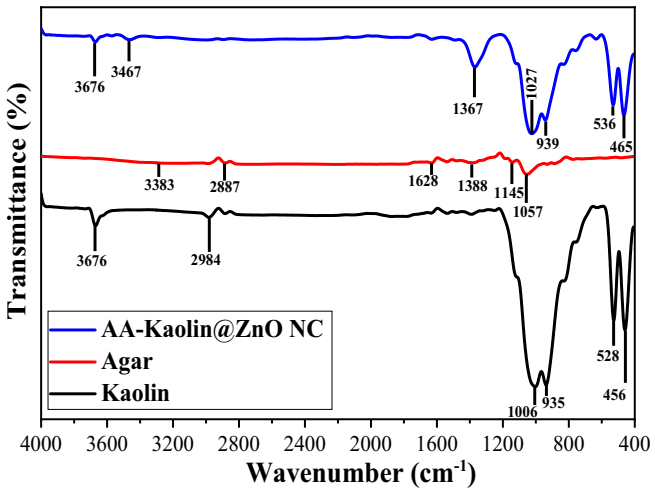

FIGURE 1 FTIR spectra of Kaolin (black line), Agar (red line), and Agar/Kao@ZnO NC.

where C_i and C_t are the initial and final concentrations of DNP after the photocatalytic experiment. The data obtained from the experiment was processed using MS Excel and Origin 9.1 software.

3 | RESULTS AND DISCUSSION

3.1 | Characterisation of Agar/Kao@ZnO NC

Fourier transform infrared spectroscopy (FTIR) analysis reveals specific absorption peaks corresponding to functional groups present in the material. Figure 1 consists of the FTIR data of Kaolin, Agar, and Agar/Kao@ZnO NC. FTIR spectra of Kaolin (black line) examined absorption peaks at 3676 (-OH stretching), 2,984 (aliphatic C-H stretching), 1,006 and 456 (Si-O-Si of tetrahedral sheet), 935 (Al-OH bending) and 528 (Si-O-Al stretching).[34] FTIR of agar (red line) examined absorption peaks at 3383 (-OH stretching), 2,887 (aliphatic -CH stretching), 1,628 (N-H stretching), 1,388 (C=O stretching), 1,145 and 1,057 (C-O-C stretching).[35] FTIR spectra of Agar/Kao@ZnO NC examine absorption peaks at 3676 (-OH stretching of Kaolin), 3,467 (-OH stretching of AA), 1,367 (C=O stretching), 1,027 (Si-O-Si), 939 (Al-OH bending), 536 (Zn-O stretching), and 465 Zn-O stretching vibrations.[36–38] These absorption peaks indicate the presence of specific functional groups within each material and provide insight into their chemical composition and bonding configurations.

The XRD analysis revealed distinct peaks for ZnO, Kaolin, and Agar/Kao@ZnO NC, indicating changes in

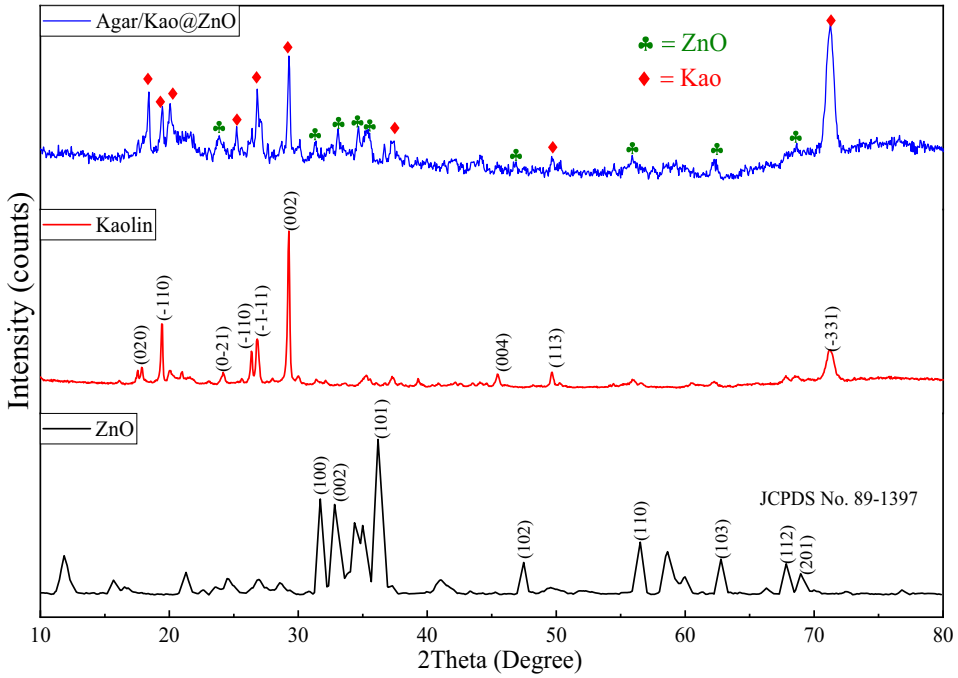

FIGURE 2 XRD spectra of ZnO NPs (black line) and Agar/Kao@ZnO NC (red line).

their solid lattice and crystalline structure as given in Figure 2. The XRD spectra of ZnO NPs (black line) displayed the characteristics peaks at 2θ values 31.90, 34.66, 36.32, 47.53, 56.41, 62.72, 67.83, 68.96 having miller indices values (100), (002), (101), (102), (110), (103), (112), and (201) according to JCPDS No. 89-1,397. The XRD spectra (red line) of kaolin exhibited the characteristic peaks around 2θ values 17.78, 24.18, 26.83, 29.25, 35.26, 35.77, 50.72, 51.42, and 71.23 corresponding to Miller indices values of (020), (−110), (0–21), (−101), (−1–11), (002), (004), (113), and (−331).[39] The XRD spectra of Agar/Kao@ZnO NC (blue line) showed peaks distinct from both ZnO and Kaolin Nanoclay. Peaks were observed at 2θ values of 18.38, 20.13, 26.07, 26.89, 29.27, 34.87, 37.49, 54.52, 63.59, and 71.23 having miller indices values (001), (011), (111), (200), (101), and (331). The quenching of the characteristic peak of ZnO in the synthesized material suggests the successful fixation of ZnO NPs in the interlayer gallery of sandwiched structured kaolin. Further information about the change in crystallite size and crystallinity upon immobilization of ZnO with kaolin and biopolymer was observed by using the Scherer formula equation (2–5).[40]

$$D = \frac{0.9\lambda}{\beta\cos\theta} \tag{2}$$

$$\text{Dislocation Density}\,(\delta) = \frac{1}{D^2} \tag{3}$$

$$\text{Interlayer Spacing}\,(d_{111}) = \frac{n\lambda}{2\text{Sin}\theta} \tag{4}$$

$$\%\text{Crystallinity} = \frac{\text{Area Under the Crystalline Peaks}}{\text{Total Area}} \times 100 \tag{5}$$

where λ is the frequency of radiation, θ is the diffraction angle, β is half the width of peaks, and D crystalline size (nm). Using equation (2–5), the XRD parameters regarding ZnO, Kaolin, and Agar/Kao@ZnO NC are given in Table 1. The Scherrer average crystallite size was calculated as 18.73 nm for ZnO NPs, 19.26 nm for kaolin, and 27.48 nm for Agar/Kao@ZnO NC. The increase in crystallite size suggests that ZnO NPs have been successfully introduced in the inlayer gallery of kaolin followed by immobilization with agar biopolymer. Further support to the formation of the material is dislocation density which is higher for the synthesized material as compared to pristine kaolin suggesting a dislocation of layers of nanoclay upon ZnO reinforcement. The dislocation resulted in interlayer spacing of 0.28 nm for Agar/Kao@ZnO NC as compared to its individual components ZnO (0.25 nm) and kaolin (0.31 nm). By using equation (5), the bulk ZnO NPs were 65.25% crystalline, kaolin was 37.91% whereas Agar/Kao@ZnO NC was 35.11% crystalline. The synthesized material has more amorphous character due to the presence of biopolymer matrix of agar which is capping the Kao@ZnO NPs.

The surface morphology of Agar/Kao@ZnO NC was analyzed using scanning microscopic technique (SEM).

TABLE 1 XRD parameter of ZnO, Kaolin, and Agar/Kao@ZnO.

Component	2θ	FWHM (β_{hkl})	Interlayer spacing (nm) at 2θ	Crystallite size (nm) at 2θ value	Dislocation density (δ) lines ($10^{19} \times m^2$)	Crystallinity (%)
ZnO	36.19	0.56	0.25	15.09	1.60	65.25
Kaolin	29.24	0.20	0.31	40.60	1.04	37.91
Agar/Kao@ZnO	29.26	0.23	0.28	36.85	1.28	35.11

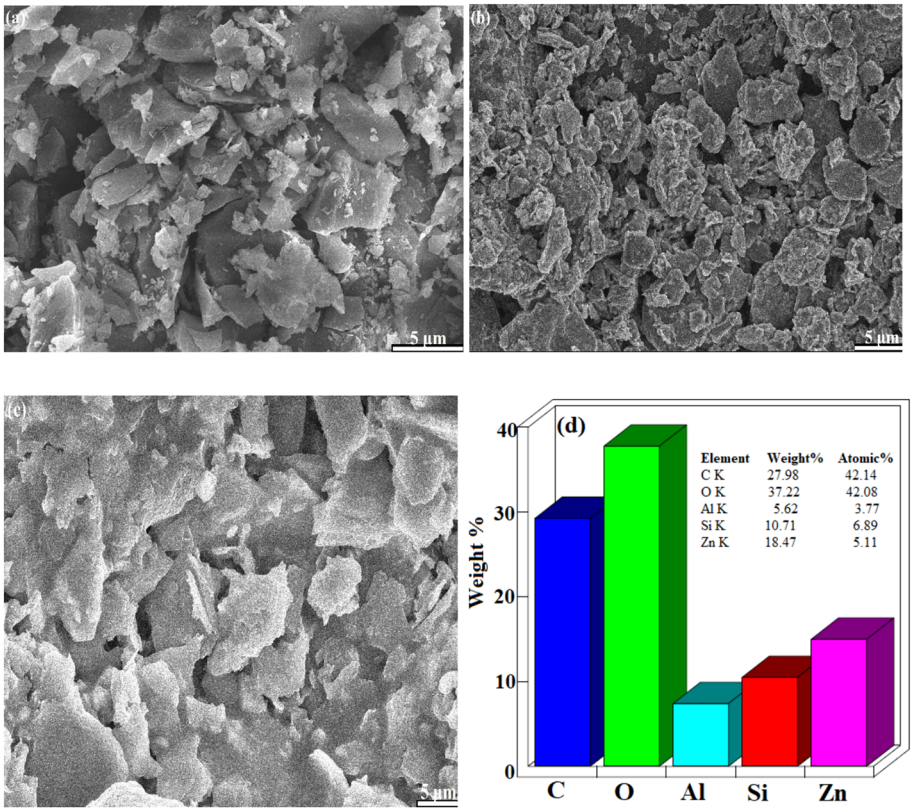

FIGURE 3 SEM images of (a) Kaolin, (b) Agar, (c) Agar/Kao@ZnO NC, and (d) EDX spectra of Agar/Kao@ZnO NC.

Figure 3a,b presents the SEM image of kaolin nanoclay with agar biopolymer which appear as flaky destacked sheets of nanoclay with irregular shape and size while agar biopolymer shows a porous and amorphous morphology. Figure 3c presents the SEM image of the Agar/Kao@ZnO NC, which appears cubical in shape with a porous surface, indicating the presence of ZnO NPs within a layer of kaolin and agar matrix. This porous surface suggests that the ZnO NPs are stabilized and supported by the functionalization of the surface. Figure 3d presents the EDX-spectra of the Agar/Kao@ZnO NC, illustrating the elemental composition of the individual component present in the material within an energy range of 1–20 keV. The weight percentage of each constituent is C (27.98%), O (37.22%), Al (5.62%), Si (10.71%), and Zn (18.47%). Figure S13d shows the distribution of elements C, O, Al, Si, and Zn, indicating that the synthesized material is pure, with no foreign elements present.

TEM analysis was conducted to further explore the morphology, particle size, and distribution in the synthesized nanocomposite material. Figure 4a presents the TEM image of Agar/Kao@ZnO NC, revealing an agglomerated spherical distribution of ZnO NPs between the sheets of Kaolin immobilized with agar biopolymer. The introduction of ZnO NPs into the Kaolin matrix is clearly depicted, resulting in the delineation of clay sheets. In Figure 4b, Gaussian profiles are depicted to show the statistical distribution of nanoparticles, resulting in an average particle size of 20 nm. Figure 4c shows the selected area diffraction pattern (SAED) of the synthesized material. The yellow diffraction fringes obtained show good agreement with XRD analysis, confirming the crystalline nature of the synthesized material and providing additional support for the structural characterization.

X-ray photoelectron (XPS) spectra were utilized to determine the chemical composition and oxidation of

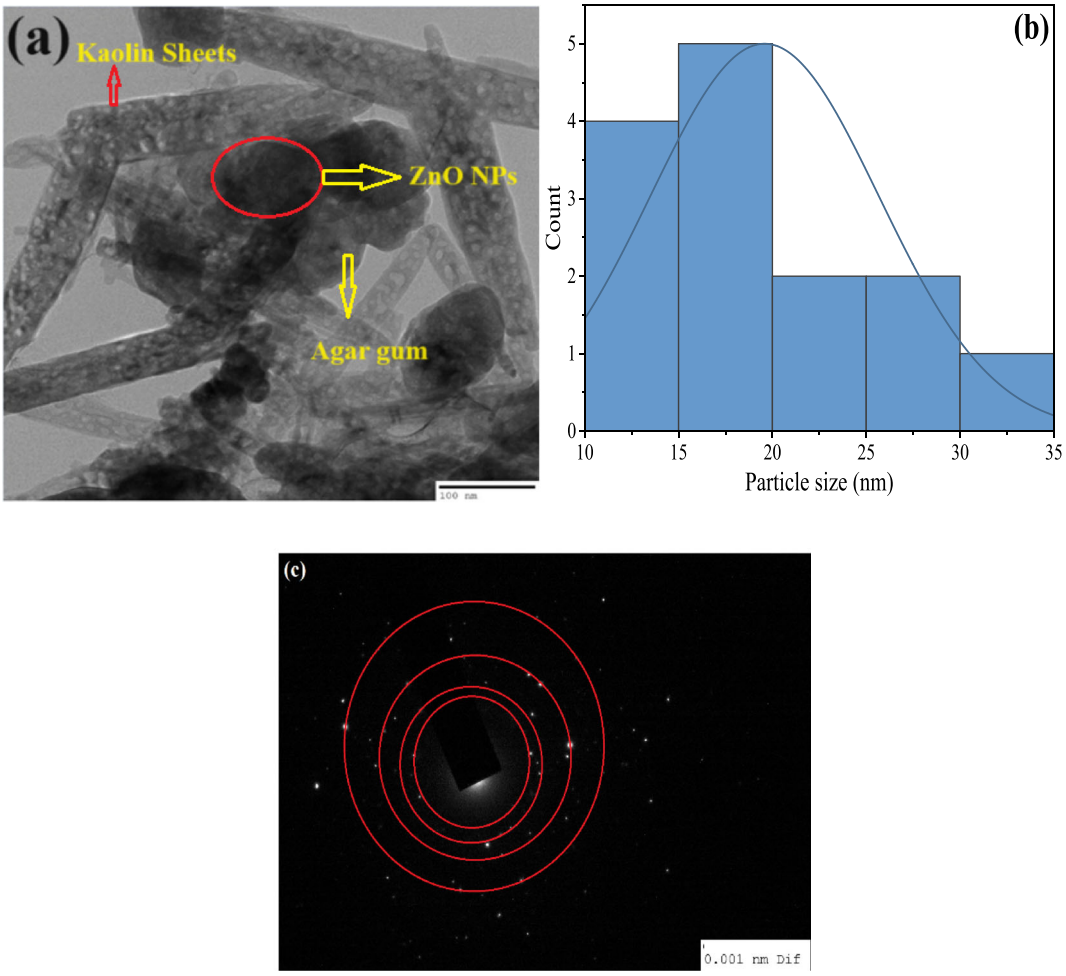

FIGURE 4 TEM image of (a) Agar/Kao@ZnO NC and (b) Gaussian distribution profile for particle size and (c) SAED image of Agar/Kao@ZnO NC.

individual elements present in the Agar/Kao@ZnO NC. Figure 5a illustrates the survey scan of Agar/Kao@ZnO NC, indicating the presence of Zn, C, O, Si, and Al in the material. Figure 5b shows the binding energy of O1s spectra with triplet peaks of 532.07 eV, 530.37 eV, and 529.09 eV corresponding to O-C-O, C-O-C/C-O-H, and C=O, respectively.[41] Figure 5c shows the binding energy of C1s spectra with triplet peaks of 283.95 eV, 285.7 eV, and 282.18 eV corresponding to C-O, C=O, and C-C/C-H, respectively, present in the material attached to kaolin and agar.[42] Figure 5d shows the binding energy of Al2p spectra at 74.27 eV and 73.18 eV corresponds to Al $2p_{1/2}$ and Al $2p_{3/2}$, respectively.[43] Figure 5e shows the binding energy of Si2p spectra at 101.7 eV, 102.7 eV, and 100.8 eV corresponding to Si-O-H, Si-O-C, and Si-O-Si, respectively.[44] The spectra of Al2p and Si2p confirm that kaolin is present in the matrix of agar biopolymer and ZnO NPs. Figure 5f shows the binding energy of Zn2p spectra at 1043.14 eV and 1020.04 eV corresponds to $Zn2p_{1/2}$ and $Zn2p_{3/2}$ form of ZnO NPs, respectively.[45,46]

The surface area and porosity of Agar/Kao@ZnO NC at low temperatures were assessed through N_2 adsorption–desorption analysis. Figure 6 illustrates the N_2 adsorption–desorption isotherm with the pores size distribution using the Barrett–Joyner–Halenda (BJH) method, revealing a mesoporous structure with a type IV shape. For synthesized material, the BET surface was determined to be 11.5 m^2/g with a pores size of 7.25 nm. Comparing this to literature values for ZnO NPs were 34.5, 27.3, 22, and 14.5 m^2/g.[47–49] It is evident that there is a decrease in the surface area of ZnO NPs in the synthesized material. This reduction suggests that the surface area of ZnO NPs has been effectively assembled and functionalized with kaolin nanoclay and agar biopolymer, contributing to the observed decrease in surface area.

Figure 7a shows the UV–Vis spectra of ZnO NPs and Agar/Kao@ZnO NC material across the wavelength range of 200–500 nm. In the UV–Vis spectrum of ZnO NPs, the absorption maxima (λ_{max}) were observed at

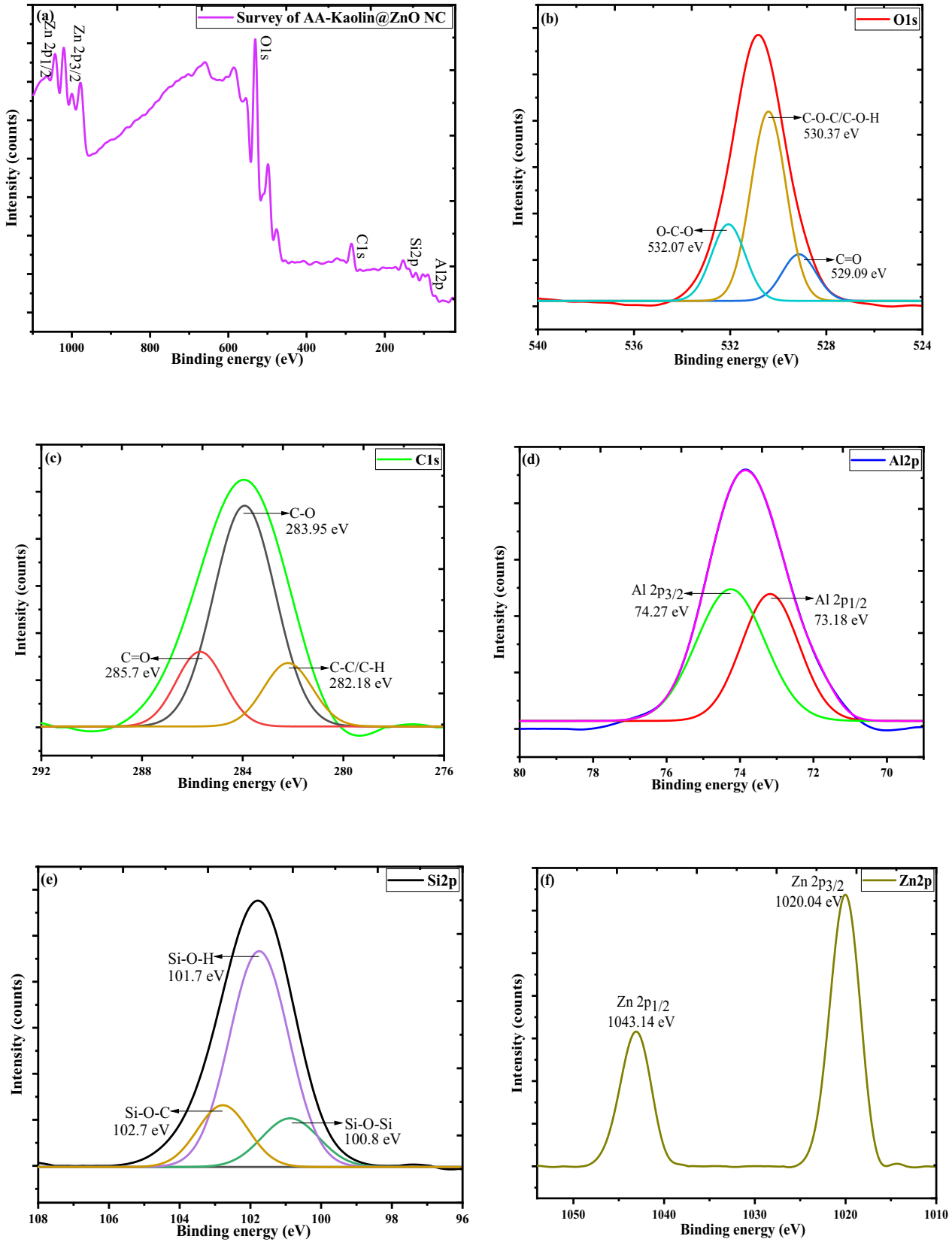

FIGURE 5 XPS spectra of (a) survey of Agar/Kao@ZnO NC, (b) O1s, (c) C1s, (d) Al2p, (e) Si2p, and (f) Zn2p.

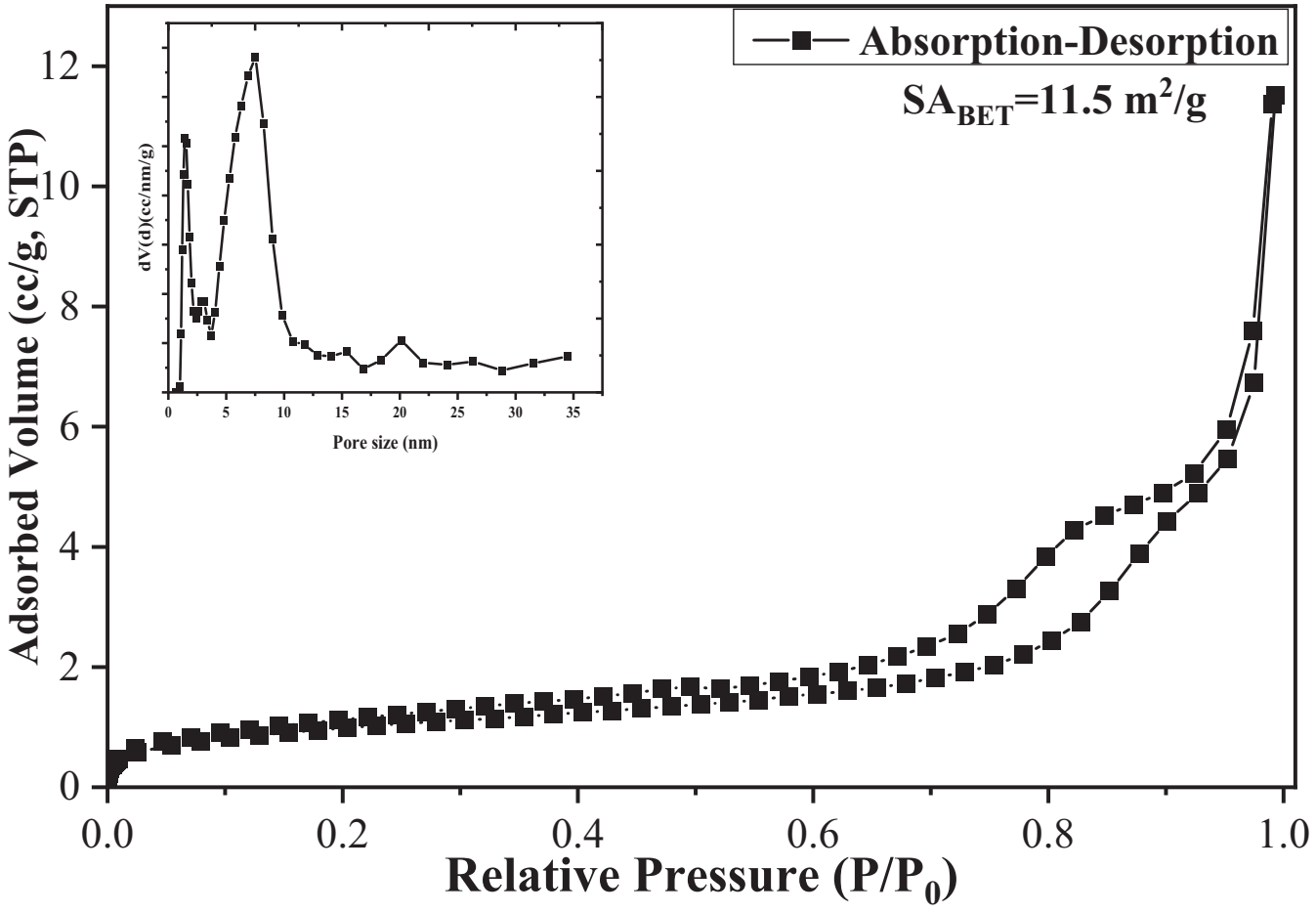

FIGURE 6 N_2 adsorption–desorption curve for Agar/Kao@ZnO NC (insert is Barrett–Joyner–Halenda (BJH) pore size graph).

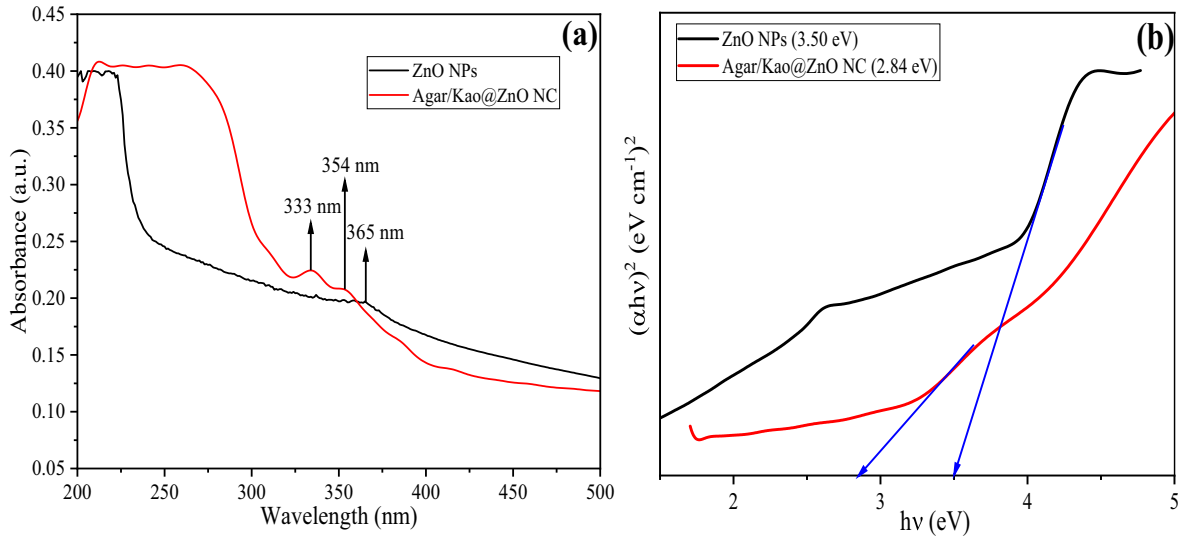

FIGURE 7 (a) The UV–vis spectra of ZnO NPs and Agar/Kao@ZnO NC material in the wavelength range of 200–500 nm and (b) corresponding Tauc's plot for observation of bandgap.

365 nm, corresponding to the characteristic peak for hexagonal wurtzite ZnO. The UV–vis spectra of the synthesized nanocomposite exhibited two absorption maxima one at 333 nm corresponding to kaolin and another 354 nm corresponding to ZnO NPs present in the matrix. The blue shift in the absorbance of ZnO NPs in Agar/

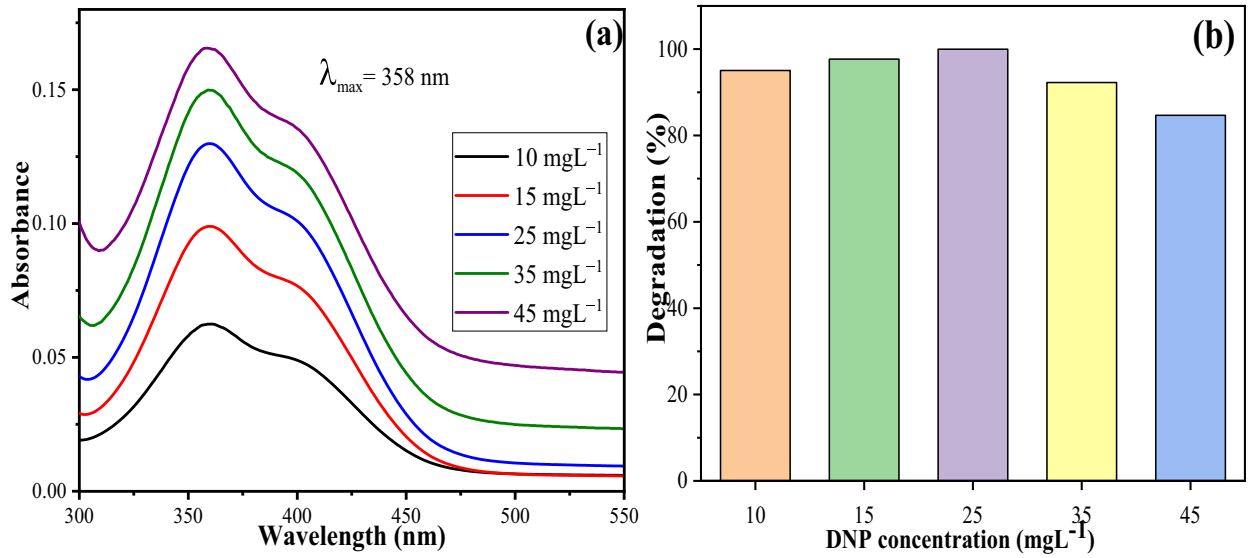

FIGURE 8 (a) Effect of initial concentration of DNP (10–45 mg L^{-1}) and (b) %degradation by using 10 mg catalyst dose in the presence of visible light source.

Kao@ZnO NC suggests the effective transformation of Zn^{2+} ions into ZnO NPs within the nanoclay matrix functionalized with biopolymer chains which is further supported by energy band gap values estimated by Tauc's plot given in inset of Figure 7b and equation (6)[50];

$$(\alpha h\nu) = A\left(h\nu - E_g\right)^n \quad (6)$$

The Tauc's plot was used to estimate the direct or indirect band energy gap values (E_g) of ZnO NPs and Agar/Kao@ZnO NC. Using Tauc's equation, the band gap value of ZnO and Agar/Kao@ZnO NC was found to be 3.50 eV and 2.10 eV. The reduction in the band gap value from 3.50 eV to 2.10 eV can be attributed to the contraction in the quantum confinement effect observed in ZnO NPs embedded within kaolin matrix and immobilized by agar biopolymer chains.

3.2 | Photocatalytic application

3.2.1 | Influence of DNP concentration

Figure 8a,b illustrates the influence of different DNP concentrations on the photocatalytic efficiency of the catalyst and rate of degradation. The investigation involved using 20 ml of aliquot of DNP solutions ranging from 10 to 50 mg L^{-1} concentration, with 10 mg of catalyst in the presence of a visible light source. It was observed that the catalyst's performance exhibited an abnormal behavior corresponding to %degradation as a function of DNP concentration. Using UV–vis curve, %degradation values of DNP for different concentrations as- 95.06%; 10 mgl^{-1}, 97.65%; 15 mgl^{-1}, 99.37%; 25 mgl^{-1}, 95.27%; 30 mgl^{-1} and 87.66%; 40 mgl^{-1}. Based on these results, the DNP concentration of 25 mg L^{-1} was chosen to be optimized concentration for further photocatalytic experiments.

3.2.2 | Influence of dosage

The influence of catalyst dosage on the degradation of DNP using BNC was examined at different catalyst dosages. Figure S1(a–c) presents the UV–vis absorption spectra for the photocatalytic degradation of DNP with respect to the irradiation time, varying catalyst dose from 10 to 20 mg. Figure 9a, plot between C_t/C_0 and time (10–50 min) is depicted for different catalyst dosages (10, 15, 20 mg) for 20 mg L^{-1} DNP concentration. The results obtained exhibited the photocatalytic efficiency of synthesized material towards DNP, yielding degradation rates of 91.51% for 10 mg; 95.58% for 15 mg; and 99.45% for 20 mg of catalyst. It can be observed that with the increase in the catalyst dose, the rate of DNP photodegradation also increases. This phenomenon can be attributed to the increasing number of active sites with higher catalyst doses, leading to a greater degree of molecular interaction between the catalyst surface and DNP molecules until the formation of adsorbate-adsorbent equilibrium. Subsequent interaction with radiation falling on the surface of the catalyst results in the formation of

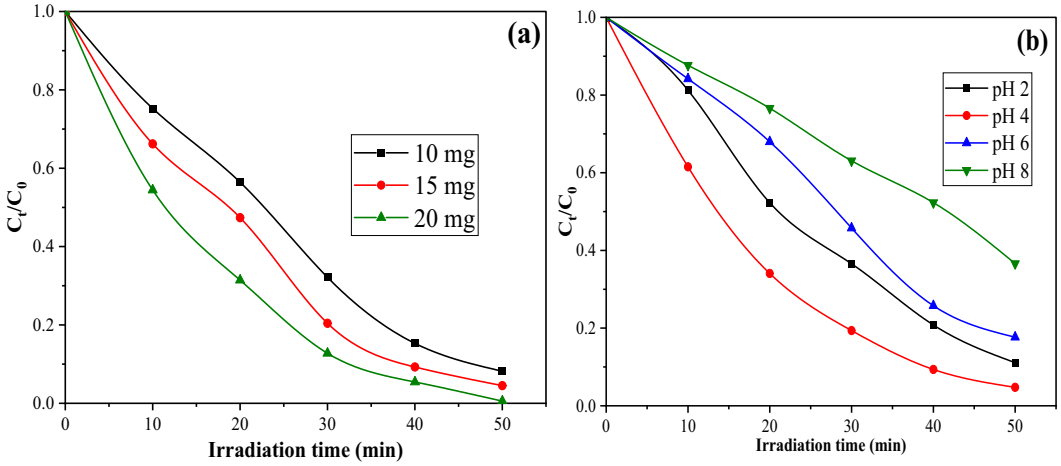

FIGURE 9 (a) C_t/C_0 graph with respect to time for the effect of different catalyst doses 10 mg, 15 mg, and 20 mg on 2,4-DNP and (b) C_t/C_0 graph with respect to time for the effect of different pH via 4, 6, 8 and 10.

photogenerated electron–hole pairs, which further generate reactive oxidant species (ROS) for the degradation of DNP.

3.2.3 | Influence of pH

The influence of pH on the photocatalytic efficiency of Agar/Kao@ZnO NC at different pH conditions i.e., 4, 6, 8, and 10 using 20 mg L^{-1} DNP with 20 mg catalyst dose for irradiation of 10–50 min. Figure S2(a–c) shows the UV–vis absorption spectra for the photocatalytic degradation of DNP at different pH values. As the irradiation time increases, the absorption values continuously decrease at each of pH values. Figure 9b presents the plot of C_t/C_0 vs time (10–50 min) from various pH values. The highest rate of degradation was achieved at pH 4 (99.26%) while the lowest at pH 8 (63.50%). This variation of photocatalytic efficiency can be explained based on the surface charge and point of zero charge (pH_{pzc}) of the NC, which is obtained as 5.15 given in Figure S3. At pH 2, surface will be highly positive, resulting in a repulsive force for OH_2^+ ionic form of DNP. Consequently, a lower number of DNP molecules will accumulate on catalyst surface, leading to reduced photocatalytic efficiency (89%). At pH 4, the positive surface of catalyst will exert an electrostatic force for phenolate anions, allowing the maximum number of DNP molecules to accumulate on the surface of the catalyst through adsorption–desorption equilibrium, resulting in maximum photocatalytic efficiency. At pH 6, the surface of the catalyst will be negative due to pH pzc value being 5.15 given in Figure S3, leading to repulsive force for phenolate anions and thus again reduced rate of DNP degradation (82.68%). Similarly, at pH 8, the magnitude of repulsive force will be greater, leading to a further decrease in photocatalytic efficiency of the catalyst.

3.3 | Kinetics of photocatalysis

The kinetics efficiency of Agar/Kao@ZnO NC and its individual constituents towards 2,4-DNP was evaluated by taking 20 mg catalyst with 25 mg L^{-1} concentration of 2,4-DNP at pH 4 for an irradiation time of 50 min. The obtained data was applied to the Langmuir-Hinshelwood (L-H) pseudo first order model given by mathematical equation (7, 8) was used[51]

$$-\ln\frac{C_t}{C_0} = kt \tag{7}$$

$$t_{1/2} = \frac{0.693}{k} \tag{8}$$

where C_0 and C_t represent the initial and final concentration of 2,4-DNP, k_1 is the rate constant and $t_{1/2}$ is half-life period.

Figure 10a presents the C_t/C_0 vs irradiation time graph for 2,4-DNP with respect to various reaction conditions like (i) DNP + light (photolysis) (ii) DNP + Catalyst+ no light (adsorption) (iii) Cat+ DNP + UV light (iv) Agar + DNP + vis light (v) Kaolin + DNP + vis light (vi) ZnO + DNP + vis light and (vi) Cat+ DNP + vis light. In the case of photolysis, the rate of DNP degradation was negligible (1.70%), indicating that DNP does not degrade spontaneously under visible light without a catalyst. During the adsorption process, the material exhibited some extent of adsorption (28%), attributed to the presence of -OH group functionalized biopolymer

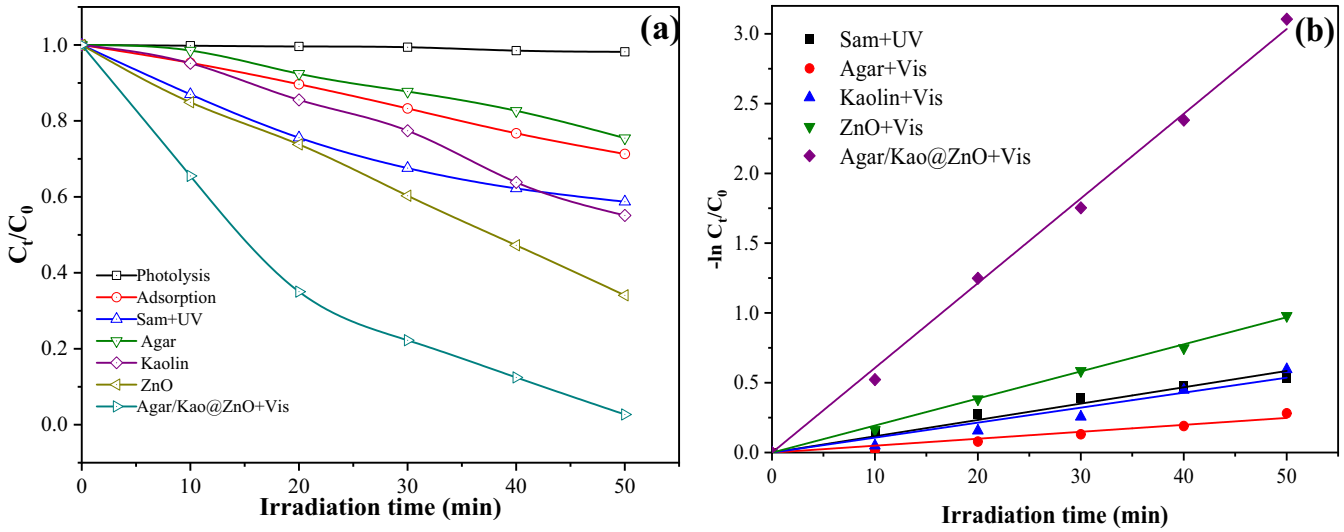

FIGURE 10 (a) C_t/C_0 and (b) -ln (C_t/C_0) with respect to irradiation time for the photocatalytic degradation of DNP by Agar/Kao@ZnO NC and its individual components at various radiation conditions.

TABLE 2 The pseudo-order reaction with kinetic parameters for the photodegradation of DNP dye by Agar/Kao@ZnO NC.

S.N.	Catalyst	Rate constant (k_1) (min^{-1})	Half-life $t_{1/2}$ (min)	R^2
1	Agar/Kao@ZnO + UV	0.012	57.75	0.991
2	Agar gum +Vis	0.0049	141.43	0.977
3	Kaolin + Vis	0.011	63.00	0.976
4	ZnO + Vis	0.019	36.47	0.987
5	Agar/Kao@ZnO + Vis	0.061	11.36	0.991

chains and interlayer gallery of the nanoclay kaolin. This adsorption process aids in the adhesion of electrically charged DNP molecules to the catalyst surface for subsequent photodegradation.

When subjected to UV light irradiation, the synthesized material demonstrated appreciable DNP degradation (41%) with an apparent rate constant value of 0.012 min^{-1} and half-life value of 57.75 min. The photocatalytic reaction rates of the Agar/Kao@ZnO NC and its constituents like agar, kaolin, and ZnO were observed toward DNP under visible light and results are summarized in Table 2. It can be seen from Figure 10a,b and Table 2 that synthesized material Agar/Kao@ZnO NC exhibited a higher rate of degradation towards DNP (99%) as compared to its individual constituents' agar (24%), kaolin (45%), and ZnO (66%). The apparent rate constant (k1) was found to be 0.0049 min^{-1} for agar, 0.011 min^{-1} for kaolin, 0.019 min^{-1} for ZnO, and 0.061 min^{-1} for Agar/Kao@ZnO NC with half-life time (t1/2) of 141.43 min, 63.00 min, 36.47 min, and 11.36 min, respectively. The kinetic results suggest that blending of ZnO with kaolin and agar results in enhanced photocatalytic activity of the semiconductor material.

3.4 | Determination of ROS and reusability test

Reactive oxidant species (ROS) such as $O_2^{-\bullet}$, $^{\bullet}OH$, h^+, and e^- are crucial in the photodegradation of organic pollutants, transforming them into non-toxic compounds. The trapping experiments were performed by taking 10 ml DNP aliquot of 25 mg L^{-1} concentration at pH 4 for 50 min with a catalyst dosage of 20 mg in the presence of a visible light source. To determine the role of specific ROS in DNP degradation, solutions of each scavenger were prepared at a concentration of 2.15mM different scavengers are isopropyl alcohol (IPA as $^{\bullet}OH$), Benzoquinone (BQ as $O_2^{-\bullet}$), acrylamide (AA as e^-), and EDTA (EDTA as h^+). Figure 11a presents the results obtained after photocatalytic reaction. It is evident that there is negligible change in the photodegradation of DNP in the presence of AA, EDTA, and BQ suggesting no involvement of e^-, h^+, and $O_2^{-\bullet}$ ROS in DNP degradation. However, the presence of IPA quenched the photodegradation efficiency from 99.53% (blank) to 65.6% (IPA) indicating that $^{\bullet}OH$ radicals play a primary role in the photocatalytic degradation of DNP.

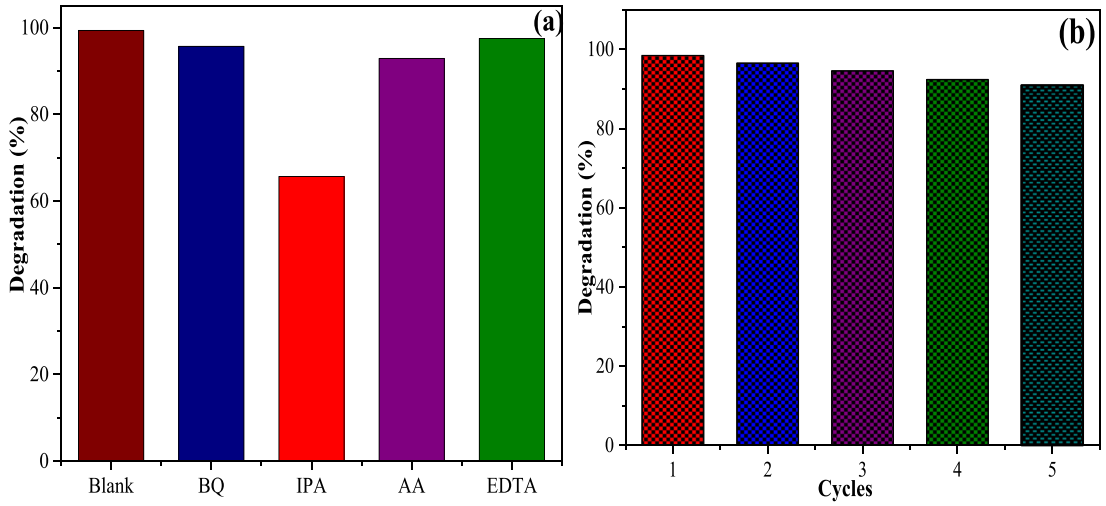

FIGURE 11 (a) Degradation (%) vs types of scavengers for determination of ROS and (b) reusability test for the determination of stability of synthesized material at the optimum value of reaction for DNP.

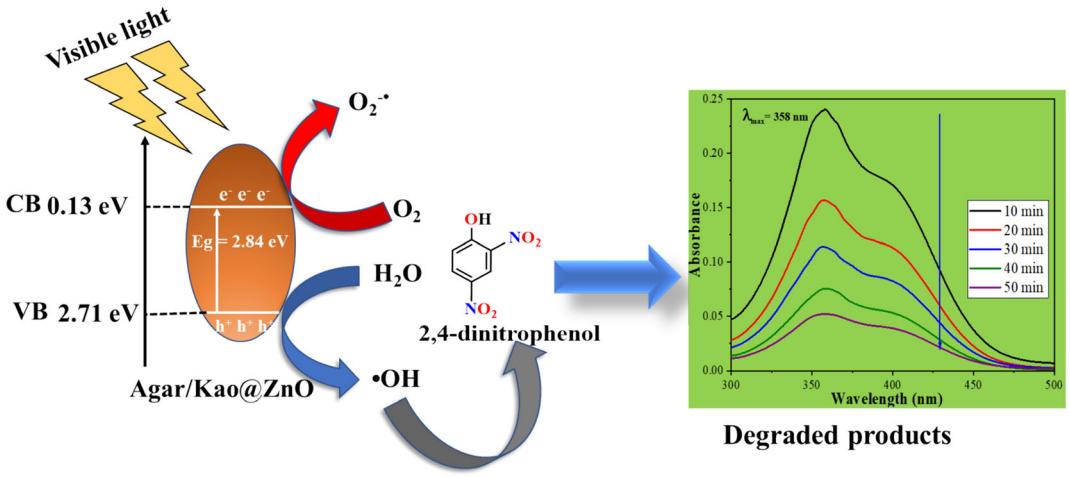

SCHEME 1 Plausible mechanism representing the photocatalytic degradation of DNP by Agar/Kao@ZnO NC.

The reusability experiment was executed to assess the stability of Agar/Kao@ZnO NC material. After completing the photocatalytic degradation of DNP, material was collected, washed with absolute ethanol, and deionized water, and dried in a hot oven. It was subsequently reused to evaluate its photocatalytic efficiency. The reusability experiment was carried out under optimized conditions, including a DNP concentration of 20 mg L^{-1}, time of 50 minutes, and catalyst dosage of 20 mg, at pH 4 in the presence of a visible light source. This experiment was repeated for five consecutive cycles, and the results are given in Figure 11b. It was found that a very appreciable change in the photocatalytic efficiency of the synthesized material occurred even after five cycles of reuse. These results suggest that the synthesized material exhibits high stability and efficient towards the degradation of DNP under the optimized reactionconditions. XRD analysis of the material was done after photocatalytic experiments and the results are given in Figure S4. It can be seen from the XRD spectra that there is no change in solid structure of the material even after five cycles of consecutive reuse. This emphasize that material is highly stable towards photocatalytic treatment of DNP.

3.5 | Mechanism of degradation

The mechanism of DNP by Agar/Kao@ZnO NC under visible light irradiation has been given in Scheme 1. Mulliken's electronegativity theory was used to calculate the

TABLE 3 Comparison data of present study with literature.

Material	Light	Concertation	Time (min)	Dosage	Degradation (%)	References
ZnO/RGO	Visible	10 ppm	75	30 mg	90.00	[54]
ZnO NPs	UV	20 ppm	60	25 mg	84.42	[55]
Ag_3PO_4/TiO_2	UV	10 ppm	60	1 g/l	96.10	[50]
Bi_2O_3 nanowires	Visible	2 ppm	300	NA	90.00	[56]
Ag_2CO_3/PSGCN	Visible	1×10^{-4} M	120	0.5 mg/ml	98.00	[57]
Agar/Kao@ZnO	Visible	25 ppm	50	20 mg	99.63	Present study

potentials of VB and CB of the synthesized material by using the following equations[52]:

$$E_{VB} = \chi - E^{(e)} + 0.5 \times E_g \quad (9)$$

$$E_{CB} = E_{VB} - E_g \quad (10)$$

where χ is Mullikens electronegativity, $E^{(e)}$ is the energy of the free electron (4.5 eV), E_g (energy bandgap of material obtained through Tauc's plot). Using equation (8, 9), the valence band (VB) and conduction band (CB) potentials of the material were found to be 2.71 eV and 0.13 eV, respectively. Since the CB potential of the synthesized material is lower than the reduction potential of oxygen ($E_0[O_2/O_2 - \bullet] = -0.33$ eV/NHE) suggesting its inability to produce $O_2 - \bullet$ radicals. While the VB potential of the material is 2.71 eV is higher than that oxidation potential of water i.e. ($E_0[H_2O/OH^\bullet] = 2.33$ eV/NHE) which can easily oxidize water molecules to hydroxyl radicals. The mechanism of photocatalytic degradation of DNP has been explained in Scheme 1. The material upon irradiation of light undergoes excitation by transferring electrons from VB to CB resulting in the formation of a photogenerated electron–hole pair. The electron in CB of the material having lower redox potential than the reduction potential of oxygen does not interact with surrounding oxygen to induce $O_2 - \bullet$ radicals. This is also supported by the scavenger experiment which shows no involvement of $O_2 - \bullet$ radicals in DNP degradation. The holes (h^+) in VB of materials having oxidation higher than oxidation protentional oxidation potential of water vs NHE interacts with surrounding water molecules resulting in the generation of highly reactive $^\bullet$OH radicals which react with DNP molecules and degrade them into nontoxic entities like CO_2 and H_2O. Importantly, the directional migration of photogenerated electrons and holes in the Agar/Kao@ZnO NC effectively prevents charge carrier recombination, thereby enhancing photocatalytic activity. The proposed reaction mechanism has been supported by liquid chromatography-mass spectra (LC–MS) analysis given in Figure S5. The LC spectra show various peaks indicating the formation of multiple side products at various time intervals corresponding to a mass spectrum composed of various side products of different masses.

The plausible mechanism involved in the photodegradation of DNP by Agar/Kao@ZnO NC is as given below[53];

$$\text{Ager/Kao-@ZnO} + hv \rightarrow \text{Ager/Kao-@ZnO}\left(h^+_{VB} + e^-_{CB}\right)$$

$$\text{Ager/Kao-@ZnO}\left(h^+_{VB}\right) + H_2O \rightarrow \text{Ager/Kao-@ZnO} + H^+ + {}^\bullet OH$$

$$DNP + {}^\bullet OH \rightarrow CO_2 + H_2O + etc.$$

3.6 | Comparison data with literature

From the literature, based on the data presented in Table 3, it can be concluded that Agar/Kao@ZnO NC exhibited superior effectiveness in the photocatalytic degradation of DNP compared to other synthesized materials. The comparison was made under various parameters including light source, concentration, time, dosage used, and percentage degradation.

4 | CONCLUSION

In the present work, ZnO NPs were doped in a kaolin clay matrix and then surface functionalized by agar biopolymer using chemical coprecipitation and solvent casting methods. The FTIR analysis reveals that the synthesized material is composed of surface hydroxyl groups which assisted in electrostatic adhesion of dye molecules under optimum pH conditions. The XRD analysis revealed that ZnO NPs have been successfully doped in kaolin matrix with a Scherer crystallite size of

27.48 nm and 35.11% crystallinity. The XPS studies revealed that each element involved in material formation exhibited the correlated chemical state with atomic % of C (27.98%), O (37.22%), Al (5.62%), Si (10.71%), and Zn (18.47%). The UV–Vis studies revealed that Agar/Kao@ZnO NC was visible light active with a direct band-gap value of 2.84 eV. The value of rate constant (k1) was found to be 0.0049 min^{-1} for agar, 0.011 min^{-1} for kaolin, 0.019 min^{-1} for ZnO, and 0.061 min^{-1} for Agar/Kao@ZnO NC, with corresponding half-life time ($t_{1/2}$) of 141.43 min, 63.00 min, 36.47 min, and 11.36 min, respectively. These kinetic results indicate that blending of ZnO with kaolin and agar enhances photocatalytic activity of the semiconductor material. The trapping experiment revealed that hydroxyl radicals (•OH) act as reactive oxidant species for the degradation of DNP under a visible light source, which was further supported by LC–MS results favoring the degradation mechanism of DNP by •OH radicals. Additionally, the material exhibited high stability and efficiency over multiple uses for photocatalytic applications. The limitation of this work is that the synthesized material was specifically efficient for DNP only whereas there is a lot of harmful and toxic dye present in the water bodies which needs treatment. So, in the future, we are going to extend the applicability of the synthesized material to multiple dye treatments and also explore its antibacterial properties.

ACKNOWLEDGEMENTS

The authors extend their thanks to Researchers Supporting Project (Ref: RSPD2024R670), King Saud University, Riyadh, Saudi Arabia. The authors appreciatively recognize Department of Chemistry, Chandigarh University Mohali for providing laboratory and infrastructure facilities.

CONFLICTS OF INTERESTS

The authors declare no conflicts of interest.

DATA AVAILABILITY STATEMENT

The data were available on request.

ORCID

Imran Hasan https://orcid.org/0000-0002-5661-0655

REFERENCES

1. Hasan I, Shekhar C, Alharbi W, Abu Khanjer M, Khan RA, Alsalme A. A highly efficient Ag nanoparticle-immobilized alginate-g-polyacrylonitrile hybrid photocatalyst for the degradation of nitrophenols. *Polymers*. 2020;12(12):3049. doi:10.3390/polym12123049
2. Bilal M, Adeel M, Rasheed T, Zhao Y, Iqbal HMN. Emerging contaminants of high concern and their enzyme-assisted biodegradation – a review. *Environ Int*. 2019;124:336-353. doi:10.1016/j.envint.2019.01.011
3. Rahmani H, Lakzian A, Karimi A, Halajnia A. Efficient removal of 2,4-dinitrophenol from synthetic wastewater and contaminated soil samples using free and immobilized laccases. *J Environ Manage*. 2020;256:109740. doi:10.1016/j.jenvman.2019.109740
4. Zhang X, Wang L, Liu C, et al. A bamboo-inspired hierarchical nanoarchitecture of ag/CuO/TiO2 nanotube array for highly photocatalytic degradation of 2,4-dinitrophenol. *J Hazard Mater*. 2016;313:244-252. doi:10.1016/j.jhazmat.2016.03.094
5. Hitam CNC, Jalil AA. A review on exploration of Fe 2 O 3 photocatalyst towards degradation of dyes and organic contaminants. *J Environ Manage*. 2020;258:110050. doi:10.1016/j.jenvman.2019.110050
6. Taddesse AM, Bekele T, Diaz I, Adgo A. Polyaniline supported CdS/CeO2/Ag3PO4 nanocomposite: an "A-B" type tandem nn heterojunctions with enhanced photocatalytic activity. *J Photochem Photobiol a Chem*. 2021;406:113005. doi:10.1016/j.jphotochem.2020.113005
7. Kadhim MJ, Mahdi MA, Hassan JJ, Al-Asadi AS. Photocatalytic activity and photoelectrochemical properties of ag/ZnO core/shell nanorods under low-intensity white light irradiation. *Nanotechnology*. 2021;32(19):195706. doi:10.1088/1361-6528/abe3b3
8. Isari AA, Hayati F, Kakavandi B, Rostami M, Motevassel M, Dehghanifard E. N, Cu co-doped TiO2@functionalized SWCNT photocatalyst coupled with ultrasound and UV waves: an effective sono-photocatalysis process for pharmaceutical wastewaters treatment. *Chem Eng J*. 2019;392:123685. doi:10.1016/j.cej.2019.123685
9. Yusuff AS, Taofeek Popoola L, Aderibigbe EI. Solar photocatalytic degradation of organic pollutants in textile industry wastewater by ZnO/pumice composite photocatalyst. *J Environ Chem Eng*. 2020;8(4):103907.
10. Li J, Lu T, Zhao Z, et al. Preparation of heterostructured ternary Cd/CdS/BiOCl photocatalysts for enhanced visible-light photocatalytic degradation of organic pollutants in wastewater. *Inorg Chem Commun*. 2020;121:108236. doi:10.1016/j.inoche.2020.108236
11. Bekele T, Mebratie G, Girma A, Alamnie G. Characterization and fabrication of p-Cu2O/n-CeO2 nanocomposite for the application of photocatalysis. *Colloids Surf a Physicochem Eng Asp*. 2024;685:133271. doi:10.1016/j.colsurfa.2024.133271
12. Byrne C, Subramanian G, Pillai SC. Recent advances in photocatalysis for environmental applications. *J Environ Chem Eng*. 2018;6(3):3531-3555. doi:10.1016/j.jece.2017.07.080
13. Alam U, Khan A, Ali D, Bahnemann D, Muneer M. Comparative photocatalytic activity of sol-gel derived rare earth metal (La, Nd, Sm and Dy)-doped ZnO photocatalysts for degradation of dyes. *RSC Adv*. 2018;8(31):17582-17594. doi:10.1039/C8RA01638K
14. Kadhim MJ, Mahdi MA, Selman AM, Al-Ani SJ, Hassan JJ, Ahmed NM. The most important parameters that affect the photocatalytic activity of ZnO nanostructures against organic dyes: a review. *Iran J Catal*. 2023;13:1-21.
15. Sanakousar MF, C.C V, Jiménez-Pérez VM, et al. Efficient photocatalytic degradation of crystal violet dye and electrochemical performance of modified MWCNTs/Cd-ZnO

nanoparticles with quantum chemical calculations. *J Hazard Mater Adv*. 2021;2:100004. doi:10.1016/j.hazadv.2021.100004

16. Chelli VR, Golder AK. Ag-doping on ZnO support mediated by bio-analytes rich in ascorbic acid for photocatalytic degradation of dipyrone drug. *Chemosphere*. 2018;208:149-158. doi:10.1016/j.chemosphere.2018.05.158
17. Bassi A, Hasan I, Qanungo K, Koo BH, Khan RA. Visible light assisted mineralization of malachite green dye by green synthesized xanthan gum/agar@ZnO bionanocomposite. *J Mol Struct*. 2022;1256:132518. doi:10.1016/j.molstruc.2022.132518
18. Wang Z, Bockstaller MR, Matyjaszewski K. Synthesis and applications of ZnO/polymer nanohybrids. *ACS Mater Lett*. 2021;3(5):599-621. doi:10.1021/acsmaterialslett.1c00145
19. Chan YY, Pang YL, Lim S, Chong WC. Facile green synthesis of ZnO nanoparticles using natural-based materials: properties, mechanism, surface modification and application. *J Environ Chem Eng*. 2021;9(4):105417. doi:10.1016/j.jece.2021.105417
20. Tun P, Wang K, Naing H, Wang J, Zhang G. Applied clay science facile preparation of visible-light-responsive kaolin-supported Ag @ AgBr composites and their enhanced photocatalytic properties. *Appl Clay Sci*. 2019;175:76-85. doi:10.1016/j.clay.2019.04.003
21. Rastegar Koohi S, Allahyari S, Kahforooshan D, Rahemi N, Tasbihi M. Natural minerals as support of silicotungstic acid for photocatalytic degradation of methylene blue in wastewater. *J Inorg Organomet Polym Mater*. 2019;29(2):365-377. doi:10.1007/s10904-018-1007-4
22. Guo C, du H, Ma Y, et al. Visible-light photocatalytic activity enhancement of red phosphorus dispersed on the exfoliated kaolin for pollutant degradation and hydrogen evolution. *J Colloid Interface Sci*. 2021;585:167-177. doi:10.1016/j.jcis.2020.11.055
23. Li X, Yang H. Pd hybridizing ZnO/kaolinite nanocomposites: synthesis, microstructure, and enhanced photocatalytic property. *Appl Clay Sci*. 2014;100:43-49. doi:10.1016/j.clay.2014.05.007
24. Li C, Zhu N, Dong X, et al. Tuning and controlling photocatalytic performance of TiO 2/kaolinite composite towards ciprofloxacin: role of 0D/2D structural assembly. *Adv Powder Technol*. 2020;1–12(3):1241-1252. doi:10.1016/j.apt.2020.01.007
25. Chen M, Yang T, Han J, et al. The application of mineral kaolinite for environment decontamination: a review. *Catalysts*. 2023;13(1):123. doi:10.3390/catal13010123
26. David C, Arivazhagan M, Mishrra A. Treatment of spent wash effluent using kaolin immobilised nano ZnO photocatalyst and material characterisation. *Indian Chem Eng*. 2019;1-12.
27. Li C, Sun L, Niu J, Reka AA, Feng P, Garcia H. Core-shell bi-containing spheres and TiO 2 nanoparticles co-loaded on kaolinite as an efficient photocatalyst for methyl orange degradation. *Cat Com*. 2023;175:106609. doi:10.1016/j.catcom.2023.106609
28. Jyoti A, Basu A, Ghosh A. Photocatalytic disinfection of multidrug resistant staphylococcus haemolyticus and Escherichia coli using visible-LED: a photochemical approach to curb nosocomial infection. *Environ Technol Innov*. 2022;27:102502. doi:10.1016/j.eti.2022.102502
29. Roy S, Rhim JW. Preparation of pectin/agar-based functional films integrated with zinc sulfide nano petals for active packaging applications. *Colloids Surf B Biointerfaces*. 2021;207:111999. doi:10.1016/j.colsurfb.2021.111999
30. Roy S, Rhim JW. Melanin-mediated synthesis of copper oxide nanoparticles and preparation of functional agar/CuO NP nanocomposite films. *J Nanomater*. 2019;2019:1-10. doi:10.1155/2019/2840517
31. Arfat YA, Ahmed J, Jacob H. Preparation and characterization of agar-based nanocomposite films reinforced with bimetallic (Ag-Cu) alloy nanoparticles. *Carbohydr Polym*. 2017;155:382-390. doi:10.1016/j.carbpol.2016.08.097
32. Selvalakshmi S, Mathavan T, Selvasekarapandian S, Premalatha M. Effect of ethylene carbonate plasticizer on agar-agar: NH4Br-based solid polymer electrolytes. *Ionics (Kiel)*. 2018;24(8):2209-2217. doi:10.1007/s11581-017-2417-y
33. Kumar S, Boro JC, Ray D, Mukherjee A, Dutta J. Bionanocomposite films of agar incorporated with ZnO nanoparticles as an active packaging material for shelf life extension of green grape. *Heliyon*. 2019;5(6):e01867. doi:10.1016/j.heliyon.2019.e01867
34. Mustapha S, Ndamitso MM, Abdulkareem AS, Tijani JO, Mohammed AK. Heliyon potential of using kaolin as a natural adsorbent for the removal of pollutants from tannery wastewater. *Heliyon*. 2019;5(11):e02923. doi:10.1016/j.heliyon.2019.e02923
35. Mokhtar A, Abdelkrim S, Sardi A, et al. Preparation and characterization of anionic composite hydrogel for dyes adsorption and filtration: non-linear isotherm and kinetics modeling. *J Polym Environ*. 2020;28(6):1710-1723. doi:10.1007/s10924-020-01719-6
36. Ariffin N *et al*. Effect of aluminium powder on kaolin-based geopolymer characteristic and removal of Cu 2 +. 1–18 (2021), doi:10.18240/ijo.2024.06.16.
37. Batterjee MG, Nabi A, Kamli MR, Alzahrani KA, Danish EY, Malik MA. Green hydrothermal synthesis of zinc oxide nanoparticles for UV-light-induced photocatalytic degradation of ciprofloxacin antibiotic in an aqueous environment. *Catalysts*. 2022;12(11):1347. doi:10.3390/catal12111347
38. Dye A. CuO nanorods immobilized agar-alginate biopolymer: a green functional material for photocatalytic degradation of. (2023).
39. Belachew N, Hinsene H. Preparation of cationic surfactant-modified kaolin for enhanced adsorption of hexavalent chromium from aqueous solution. *Appl Water Sci*. 2020;1–8(1):38. doi:10.1007/s13201-019-1121-7
40. Hasan I, Bassi A, Alharbi KH, Binsharfan II, Khan RA, Alslame A. Sonophotocatalytic degradation of malachite green by nanocrystalline chitosan-ascorbic acid@ NiFe2O4 spinel ferrite. *Coatings*. 2020;10(12):1200. doi:10.3390/coatings10121200
41. Wang Y, Dong X, Zhao L, et al. Facile and green fabrication of carrageenan-silver nanoparticles for colorimetric determination of Cu2+ and S2−. *Nanomaterials*. 2020;10(1):83. doi:10.3390/nano10010083
42. Gupta SSR, Kantam ML. Finely dispersed CuO on nitrogen-doped carbon hollow nanospheres for selective oxidation of sp3 C–H bonds. *New J. Chem*. 2021; 45:16179-16186. 10.1039/d1nj02406j.
43. Kloprogge JT, Wood BJ. Systematic XPS study of gallium-substituted boehmite. *J Mater Sci*. 2016;51(11):5436-5444. doi:10.1007/s10853-016-9847-1

44. Sun Z, Zhang X, Dong X, et al. Hierarchical assembly of highly efficient visible-light-driven Ag/g- C 3 N 4/kaolinite composite photocatalyst for the degradation of ibuprofen. *J Mater*. 2020;6: 582-592.
45. Le TK, Nguyen TM, Nguyen HT, et al. Enhanced photocatalytic activity of ZnO nanoparticles by surface modification with KF using thermal shock method. *Arab J Chem*. 2017;13(1): 1032-1039. doi:10.1016/j.arabjc.2017.09.006
46. Huang D, Zhang Y, Zhang J, Wang H, Wang M. The synergetic effect of a structure-engineered mesoporous SiO(2)-ZnO composite for doxycycline adsorption. 2019;9(66, 66):38772-38782. doi:10.1039/c9ra08106b
47. Man MT, Kim J, Jeong MS, Do AT, Lee HS. Author' s accepted manuscript oriented ZnO nanostructures and their application oriented ZnO nanostructures and their application in photocatalysis. *JOL*. 2016;185:17-22. doi:10.1016/j.jlumin.2016.12.046
48. Wang J, Xia Y, Dong Y, Chen R, Xiang L, Komarneni S. Defect-rich ZnO nanosheets of high surface area as an efficient visible-light photocatalyst. *Appl Catal Environ*. 2016;192:8-16. doi:10.1016/j.apcatb.2016.03.040
49. Moradi M, Hasanvandian F, Isari AA, Hayati F, Kakavandi B, Setayesh SR. Environmental CuO and ZnO co-anchored on g-C 3 N 4 nanosheets as an affordable double Z-scheme nanocomposite for photocatalytic decontamination of amoxicillin. *Appl Catal Environ*. 2021;285:119838. doi:10.1016/j.apcatb.2020.119838
50. Amiri F, Dehghani M, Amiri Z, Yousefinejad S, Azhdarpoor A. Photocatalytic degradation of 2, 4-dichlorophenoxyacetic acid from aqueous solutions by Ag3PO4/TiO2 nanoparticles under visible light: kinetic and thermodynamic studies. *Water Sci Technol*. 2021;83(12):3110-3122. doi:10.2166/wst.2021.193
51. Bassi A, Kanungo K, Heun B, Hasan I. Cellulose nanocrystals doped silver nanoparticles immobilized agar gum for efficient photocatalytic degradation of malachite green. *Int J Biol Macromol*. 2023;244:125221. doi:10.1016/j.ijbiomac.2023.125221
52. Bekele T. Synthesis and characterization of CeO2/Ag3PO4p-n heterojunction photocatalyst: its photocatalytic activity for the degradation of alizarin yellow dye. *J Nanomater*. 2023;2023:1-16. doi:10.1155/2023/7140181
53. Nguyen SN, Truong TK, You SJ, Wang YF, Cao TM, Pham VV. Investigation on photocatalytic removal of NO under visible light over Cr-doped ZnO nanoparticles. *ACS Omega*. 2019;4(7): 12853-12859. doi:10.1021/acsomega.9b01628
54. Botsa SM, Subbarao SP, Chug S. Visible light enhanced photocatalytic degradation of 2, 4-dinitrophenol using reduced graphene oxide based zinc oxide nanocomposite via hydrothermal process. 3–9 (2019) doi:10.15436/2377-1372.19.1966.
55. Nouri-Mashiran M, Taghavi L, Fataei E, Ebrahimzadeh-Rajaei G, Ramezani M. Green synthesis of ZnO nanoparticles and comparison of 2, 4-dinitrophenol removal efficiency using photocatalytic, sonocatalytic, and adsorption processes. *Main Group Chem*. 2022;21(2):559-575. doi:10.3233/MGC-210152
56. Chouke PB, Dadure KM, Potbhare AK, et al. Biosynthesized δ-Bi2O3 nanoparticles from Crinum viviparum flower extract for photocatalytic dye degradation and molecular docking. *ACS Omega*. 2022;7(24):20983-20993. doi:10.1021/acsomega.2c01745
57. Raizada P, Sudhaik A, Singh P, Shandilya P, Thakur P, Jung H. Visible light assisted photodegradation of 2,4-dinitrophenol using Ag2CO3 loaded phosphorus and sulphur Co-doped graphitic carbon nitride nanosheets in simulated wastewater. *Arab J Chem*. 2020;13(1):3196-3209. doi:10.1016/j.arabjc.2018.10.004

SUPPORTING INFORMATION

Additional supporting information can be found online in the Supporting Information section at the end of this article.

How to cite this article: Hasan I, Bassi A, Kalakonda P, Kanungo K. ZnO-doped kaolin nanoclay immobilized agar biopolymer for 2,4-dinitrophenol photocatalytic degradation. *Asia-Pac J Chem Eng*. 2024;e3144. doi:10.1002/apj.3144